Princeton Plasma Physics Laboratory

PPPL- 4554

PPPL- 4554

Optimizing Laser-accelerated Ion Beams for a Collimated Neutron Source

C.L. Ellison and J. Fuchs

September, 2010

Prepared for the U.S. Department of Energy under Contract DE-AC02-09CH11466.

Princeton Plasma Physics Laboratory
Report Disclaimers

Full Legal Disclaimer

Trademark Disclaimer

PPPL Report Availability

Princeton Plasma Physics Laboratory:

http://www.pppl.gov/techreports.cfm

Office of Scientific and Technical Information (OSTI):

http://www.osti.gov/bridge

Related Links:

U.S. Department of Energy

Office of Scientific and Technical Information

Fusion Links

Optimizing laser-accelerated ion beams for a collimated neutron source

C. L. Ellison [1] and J. Fuchs [2]

[1] *Princeton University Plasma Physics Laboratory,P.O. Box 451, Princeton, NJ 08543, USA*

[2] *Laboratoire pour l'Utilisation des Lasers Intenses, UMR 7605 CNRS-CEA-École Polytechnique-Université Paris VI, 91128 Palaiseau, France*

High-flux neutrons for imaging and materials analysis applications have typically been provided by accelerator- and reactor-based neutron sources. A novel approach is to use ultra-intense (>10^{18}W/cm^2) lasers to generate picosecond, collimated neutrons from a dual target configuration. In this article, the production capabilities of present and upcoming laser facilities are estimated while independently maximizing neutron yields and minimizing beam divergence. A Monte-Carlo code calculates angular and energy distributions of neutrons generated by D-D fusion events occurring within a deuterated target for a given incident beam of D+ ions. Tailoring of the incident distribution via laser parameters and microlens focusing modifies the emerging neutrons. Projected neutron yields and distributions are compared to conventional sources, yielding comparable on-target fluxes per discharge, shorter time resolution, larger neutron energies and greater collimation.

I. INTRODUCTION

Neutron production facilities provide a valuable resource for detailed materials analysis and imaging. Conventionally, the neutrons have been generated using fission reactions (such as the High-Flux Isotope Reactor) or by accelerating protons to spallate neutrons from a target (eg. the Spallation Neutron Source). While providing adequately large neutron fluxes, both of these methods suffer from unused neutrons scattered into large solid angles and limited temporal resolution.

Recently, the ultra-intense laser community has exhibited interest in generating neutrons at laser facilities. Experiments have measured neutron production from $D(d,n)^3He$ reactions [1,2,3] while simulations have been performed to model the reactions and assess production capabilities [4,5,6,7]. The benefits of laser-based sources include collimated neutrons, fine temporal resolution, and the ability to tailor beam properties at the time of generation. Additionally, the larger neutron energies accessible expand potential applications, for instance to fusion materials testing [8].

Previous studies have investigated the laser parameter space [4,9] and consequences of target configuration [5]. The dual target configuration (as seen in Fig. 1) has been proposed for the ability to tailor the incoming D+ ions to improve the generated neutrons. The primary deuterated target absorbs the laser pulse, and D+ ions are emitted due primarily to rear-side acceleration. The ions then impinge upon the secondary, deuterated target where $D(d,n)^3He$ fusion events produce neutrons.

In this study, we optimize the incident D+ ions first to maximize the total neutron yield and second to minimize the neutron divergence. Both optimizations are performed within the confines of present or near-future capabilities. A Monte-Carlo method similar to previous studies [4,5,6,7,10] propagates the incident ions into the secondary CD_2 target and calculates the neutron yield. Incident beam distributions are based on present laser facilities and scaling

studies for future facilities. Novel techniques such as microlens focusing [11] are proposed to obtain the desired ion beam parameters, such as a narrow energy spectrum. The optimizations are framed within the context of monoenergetic limits. We find a high degree of collimation with slightly reduced on-target fluxes compared to conventional neutron production methods.

II. CALCULATION METHODS

Neutron yields from the dual target configuration are calculated in a similar manner to previous studies [4,5,6,7,10]. The model uses a Monte-Carlo method by randomly selecting individual deuterium ions from the specified incident ion spectrum. The ion is then propagated through the secondary target and contributions the neutron spectrum are tallied based on reaction cross sections and material stopping powers. The process is repeated many times to determine the average neutron yield for a given distribution of incident ions.

To simplify the calculations, we assume: 1) the incident beam of ions exhibits azimuthal symmetry about the axis perpendicular to the secondary target, 2) a straight-line ion trajectory, and 3) neutron production is dominated by $D(d,n)^3He$ fusion events. Assumption number one is justified by the symmetry of the laser pulse incident upon the uniform target, and from this assumption we may further deduce that the emitted neutron spectrum will similarly exhibit azimuthal symmetry. The straight-line trajectory assumption has been shown in Ref. [10] to be a reasonable approximation. Finally, the consideration of neutron generation by means other than D-D fusion events has been explored by Toupin *et. al* [4]. The $^{12}C(d,n)^{13}N$ reaction was found to be the dominant of those investigated, including D-D breakup and electrodisintegration, yet non-D-D neutron generation amounted to only a few percent of the total flux at incident ion energies of tens of MeV.

The incident deuterium spectrum is not simulated by the program, but rather is taken as an input parameter. This allows for the large variety of sources to be tested, and we utilize past results [12,13] for the spectra. Approximately 10^5 randomly selected ions are propagated

through the target to sufficiently resolve the incident spectrum, which includes the energy and angular distributions of the ions. Typically, the angle is chosen according to the fraction of front-surface acceleration (FSA) vs. rear-surface acceleration (RSA) ions. FSA ions, accelerated by the electric field of the laser impinging upon the target, exhibit large angular spread compared to the narrow RSA ions, accelerated by an electric field established by the electrons exiting the rear surface of the target [12]. The angular scaling as a function of energy was studied in Ref. [14].

As the incident deuterium ion penetrates a distance dx into the target, the neutron flux contribution over that distance is given by [4,6]:

$$\Delta\left(\frac{dY_n(\alpha_n)}{d\Omega_n}\right) = n_D \frac{d\sigma(E_i,\theta_n)}{d\Omega_n} dx \quad (1)$$

Where $\left(\frac{dY_n(\alpha_n)}{d\Omega_n}\right)$ is the differential neutron yield per sterradian as a function of angle α_n with respect to the target normal, n_D is the density of deuterium atoms in the target, and $\frac{d\sigma(E_i,\theta_n)}{d\Omega_n}$ is the differential cross section as a function of ion energy and θ_n, the angle between the ion and neutron. In the same distance dx, the ion also loses energy according to the stopping power of the material:

$$\Delta E_i = S(E_i)dx\,. \quad (2)$$

The stopping power as a function of ion energy, $S(E_i)$ is presented in Ref. [15]. For the differential cross section, angular distributions are provided in Ref. [16]. The cross sections are presented for each angle between 0° and 180° in 5° intervals and for incident ion energies between 0.156 and 13.8 MeV. For plots of the cross sections and stopping power, see Ref. [10].

Finally, the energy of a neutron emitted in a general direction is calculated and recorded as dictated by 2-D kinematics. For a given ion energy E_i and a given angle of neutron emission

θ_n referenced with respect to the incident ion direction, the energy of the emitted neutron is given by [4,6]:

$$E_n = \frac{1}{8} E_i (\sqrt{2 + 19.6MeV / E_i + \cos^2 \theta_n} + \cos\theta_n)^2 . \quad (3)$$

Where E_n is taken to be in the laboratory frame, not the center of mass frame. Tallying the neutron production across the incident ion spectrum yields the neutron flux as a function of angle and energy. Azimuthal symmetry dictates that only the angle relative to the target normal is significant.

III. MAXIMIZING YIELDS

A. Neutrons per Ion

To establish a base for comparison for the experimental ion distributions and to confirm agreement with past results, the simplified case of monoenergetic, normally incident ions was calculated for a set of energies varying from 0.1 MeV to 10 MeV. Secondary CD_2 target thickness was set to 25mm to fully stop the incident ions and maximize total yield. The angular distributions presented in these results serve as a useful guide for understanding the neutron production on a per-ion level. The maximum yields for monoenergetic ions may be linearly scaled to the total incident particles, and we gain a sense for the degree of collimation of the neutrons which cannot be exceeded for a given energy due to the geometry of the energy-angle cross sections. At 0.1 MeV, we find 6.8 x 10^{-8} n/ion, 1 MeV yields 8.8x10^{-6} n/ion, and 10 MeV yields 5.1 x 10^{-4} n/ion, in reasonable agreement with [10]. In the forward direction, the yields are calculated to be 0.1 MeV – 1.0x10^{-8} n/sr/ion, 1 MeV – 2.2x10^{-6} n/sr/ion, 10MeV – 4.3x10-4 n/sr/ion, which match the results in [4]. The angular yields per ion for incident energies between 0.1 MeV and 10 MeV are presented in Fig. 2.

From this figure, the increasing anisotropy of the neutron emission may be observed. At higher energies, the beam becomes significantly more collimated. Moreover, the increased

neutron yield per ion at greater energies indicates the significance of the high energy portion of the incident spectrum. As such, the neutron emission is expected to be sensitive to the characteristics of the high energy tail.

B. Present Facilities

The distribution of protons accelerated from thin metal targets has been studied in past experiments at the 100 TW Laboratoire pour l'Utilisation des Lasers Intenses (LULI) and 30 TW Trident laser facilities [12]. Both lasers provided 20-30 J of beam energy at a wavelength of 1.057 μm. We match a hypothetical deuterium spectrum to the reported proton spectra. The neutron production code allows extrapolating the possible neutron production if the emitted ion spectrum were to impinge upon a secondary CD_2 target. The original plots representing the spectrum are shown in Ref. [12].

Using these input ion distributions, the Monte-Carlo code calculated the resulting neutron spectra as a function of energy and angle, again using a 25mm thick secondary target. Figure 3 presents the results. The angular distribution of the emitted neutrons is presented in a polar plot and energy distributions in the forward and perpendicular direction (referenced with respect to the incident ion beam) are plotted.

With an incident laser intensity of 1×10^{19} W/cm^2, the total neutron yield is estimated to be 1.8×10^{7} neutrons emitted by the 6.2×10^{11} incident deuterium ions. For $I = 6\times10^{19}$ W/cm^2, the total yield is 2.5×10^{7} from the 6.8×10^{10} incident ions. The increased number of neutrons per ion in the latter case aligns with expectations of increased neutron yield due to the higher energy portion of the incident ion spectrum. The latter case also exhibits higher energy neutrons and greater collimation. These yields align with experimental studies which have measured 10^4 – 10^7 neutrons per joule of laser energy [1-3].

C. Future Capabilities

The most direct way to maximize neutron flux is to increase deuteron yields and energies. Next generation laser facilities, such as the Extreme Light Infrastructure (ELI) [17], are designed to enhance both of these parameters. Extrapolations have been performed to predict proton production from ultra-intense laser interactions with thin targets [13]. This study calculated maximum ion energy for the given laser facilities, and from them we may model the ion distribution spectrum using the model described in Ref. [18]. The spectra may be calculated for a wide range of upcoming laser parameters. We present neutron yield calculations in an extreme and moderate case.

For the extreme case of a laser energy of 2 kJ and intensity of $I = 1.6\times10^{23}$ W/cm^2, the ion spectrum has been determined using the method described in Ref. [18]. We find a total of 1.3×10^{13} ions accelerated from the target. Similarly, the moderate case involved a laser intensity of 1.6×10^{21} W/cm^2 and 1.1×10^{13} incident ions.

Similar to previous spectra, the number of ions decreases monotonically with increasing energy. With energies on the order of hundreds of MeV, targets are no longer thick enough to fully stop the incident ions. A 10 MeV ion will stop within a 1 mm target, but fully stopping ions on the order of 100 MeV would require unrealistically large CD_2 targets. As such, the emitted neutron spectrum will be less sensitive to properties in the tail of the spectrum since most particles escape before depositing all of their energy into the target.

Figure 4 presents the expected neutron emission available at the ELI facility. Integrating this angular distribution, we find a total of 10^{11} emitted neutrons from D-D fusion events. Now, this projection involves additional caveats which increase the uncertainty compared to the current facility projections. Namely, the D-D cross section data, especially the angularly resolved data, is unavailable at such high incident energies. As such, the calculations are performed using cross section data from below 100 MeV, which may be inaccurate. Additionally, alternative reactions may increase to become non-negligible.

These limitations aside, the calculations provide useful order-of-magnitude estimates of the total neutron production. These estimates are useful in comparison with previous studies and conventional means of producing neutrons. While the angular distribution may not be as accurate as those presented at lower energies, the increasing anisotropy with incident ion energy suggests high degrees of collimation persisting even at higher energy levels, and we estimate neutron production on the order of 10^{11} neutrons were the dual target configuration implemented at the ELI facility. Moreover, increasing contributions from non-DD fusion events may compensate for the presumably decreasing DD cross section.

IV. MINIMIZING NEUTRON SPREAD

Instead of maximizing the total number of neutrons, the application of the neutrons may demand a narrow energy or temporal spectrum. Modifications to the incident ion spectrum and target configuration allow minimizing spatial and temporal divergence of the beam. Any spread in the energy of the neutrons generated in the secondary target will propagate as a spatial distribution as the neutrons move away and a temporal spread at the target. We explore two methods of mitigating this effect: thin secondary targets and microlens as shown in Fig. 5. Thin targets eliminate the lower energy (and less collimated) neutrons from ion slowing in the target while microlens energy selection diminishes the time of flight spread between the primary and secondary targets. The methods are studied individually, and are found to enhance neutron collimation at the cost of diminished total yields.

A. Monoenergetic Limits

To determine fundamental limits on narrowing the neutron spectrum, we return to the case of monoenergetic deuterium ions. This time, however, we limit the secondary target thickness to 20 microns instead of 25 mm. Neutron production is still dominated by high energy deuterons but the deuterons exit the target before depositing all of their energy, reducing the

neutron energy spread. Figure 6 shows the compact energy spectrum resulting from the thin secondary target modification. Only energy distribution plots are shown since the angular distributions highly resemble those in Fig. 2. The narrowing of the energy spectrum in the thin target configuration is immediately apparent in Fig. 2. As a tradeoff, the total yield decreases since the ions do not deposit all of their energy. This becomes more severe at higher energies. For instance, the total yield from 1 MeV is largely unchanged at 8.8×10^{-6} n/ion, but at 10 MeV a 98% decrease from 5×10^{-4} to 1×10^{-5} n/ion is observed. The impact on temporal spread at the imaging target is significant, however. The presence of neutrons with energies between 4 MeV and 10 MeV in the thick target, 10 MeV ions scenario equates to a 50μs separation at a 1m distant target, negating the benefits of picosecond scale neutron generation. With the thin target, a .2 MeV spread about a central peak of 10 MeV reduces the temporal separation at 1m to 200 ps.

B. Microlens Filtering

Energy selection techniques may be used to narrow the incident ion spectrum, providing an effective means of collimating the emergent neutron spectrum when combined with thin secondary targets. While conventional energy selection methods exist, we propose implementing the methods discussed in Ref. [11] where energy filtering of the incoming deuteron beam is made possible by exciting strong electric fields in circular cavities which the ion beam passes through. A schematic of this configuration is shown in Figure 5. To model this effect, a function was implemented in the calculation code which modified the incident deuteron spectrum to mimic the results of a microlens filter. The artificial microlens filter was set to amplify a central energy while quickly dropping off in either direction. Energies below a few ``widths'' (typically .1MeV) of the central energy are set to zero incident deuterons while

energies above return to their original values. This replicates the high energy deuterons passing through the microlens before the focusing pulse arrives.

The energy selection criteria was applied in conjunction with the thin target configuration to the 6×10^{19} W/cm^2 LULI spectrum and the moderate ELI case used in Sec. III. The central peaks were chosen to be 12 MeV for the LULI spectrum and 200 MeV for the ELI spectrum. The total neutron yield in the former dropped to 1.4×10^5 neutrons in the LULI calculation and 1.4×10^8 in the ELI calculation due to the fewer incident ions. The incident spectra and emerging energy spectra are presented in Fig. 7. The neutron energy spectrum is observed to be extremely narrow due to the focused ion beam. Experimental implementation of the microlens technique is likely to provide an effective means of achieving nearly monoenergetic neutrons.

V. CONCLUSION

The ability to create neutrons at ultra-intense laser facilities expands the capabilities of neutron characteristics beyond those available at conventional sources. Primarily, the collimated beam of neutrons and short time resolution stand in stark contrast to the steady-state, isotropic sources. The collimation relaxes shielding requirements and indicates that for a given amount of total neutrons, a higher fraction will be available as on-target neutrons. The short time scale of the laser pulse and minimal energy spread of the neutrons introduce the possibility of performing high time resolution measurements.

Unfortunately, not all of these advantages are exploitable across all measurement applications. For instance, lower energy neutrons are often desired for imaging purposes. While the neutrons generated by ultra-intense lasers may be cooled to adapt to low energy imaging requirements, the cooling process would make the collimated beam isotropic.

For convenient comparison of neutron sources, Table 1 has been compiled. To convert all sources to the same dimensions, the final three entries assumed a source 1m away from the target with a 20° divergence of the neutrons from the source. The LULI facility was assumed to

have a repetition rate of 1 Hz where as the high power (ELI) facility was assumed to have a rep rate of 1/60 Hz.

In comparison to conventional sources, the prospect of collimation and time resolution combined with the relative simplicity of the apparatus may make ultra-intense generated lasers an attractive alternative for some research groups. Current laser facilities are capable of delivering 10^7 neutrons, and projected scalings suggest future facility yields of 10^{11} neutrons. Spatial collimation mitigates the stringent shielding requirements of isotropic neutron sources. Further advances in target technology (such as the results presented in Ref. [19]) and laser-target interaction physics are likely to propel neutron yields beyond these predictions, making laser-based neutron sources increasingly attractive alternatives.

ACKNOWLEDGEMENT

This work was completed during the Department of Energy École Polytechnique – Princeton Plasma Physics Laboratory Exchange Program.

References

1 L. Disdier, J-P. Garconnet, G. Malka, and J-L. Miquel, Phys. Rev. Lett. **82**, 1454 (1999).

2 A. Youssef, R. Kodama, H. Habara, K.A. Tanaka, Y. Sentoku, M. Tampo, and Y. Toyoma, Phys. Plasmas **12**, 110703 (2005).

3 D. Hilscher, O. Berndt, M. Enke, U. Jahnke, P.V. Nickles, H. Ruhl, and W. Sander, Phys. Rev. E **64**, 016414 (2001).

4 C. Toupin, E. Lefebvre, G. Bonnaud, Phys. Plasmas **8**,1011 (2001).

5 G.M. Petrov and J. Davis, Phys. Plasmas **15**, 073109 (2008).

6 N. Izumi, Y. Sentoku, H. Habara, K. Takahashi, F. Ohtani, T. Sonomoto, R. Kodama, T. Norimatsu, H. Fujita, Y. Kitigawa, K. Mima, K.A. Tanaka, and T. Yamanaka, Phys. Rev. E **65**, 036413 (2002).

7 H. Habara, R. Kodama, Y. Sentoku, N. Izumi, Y. Kitagawa, K.A. Tanaka, K. Mima and T. Yamanaka, Phys. Rev. E **69**, 036407 (2004).

8 L.J. Perkins, B.G. Logan, M.D. Rosen, M.D. Perry, T. Diaz de la Rubia, N. M. Ghoniem, T. Ditmire, P.T. Springer, S.C. Wilks, Nuclear Fusion **40**, 1 (2001).

9 J. Davis and G.M. Petrov, Phys. Plasmas **15**, 083107 (2008).

10 J. Davis and G.M. Petrov, Plasma Phys. Control. Fusion **50**, 065016 (2008).

11 T. Toncian, M. Borghesi, J. Fuchs, E. d'Humières, P. Antici, P. Audebert, E. Brambrink, C.A. Cecchetti, A. Pipahl, L. Romagnani, and O. Willi, Science **312**, 410 (2006).

12 J. Fuchs, Y. Sentoku, S. Karsch, J. Cobble, P. Audebert, A. Kemp, A. Nikroo, P. Antici, E. Brambrink, A. Blazevic, E.M. Campbell, J. C. Fernández, J.-C. Gauthier, M. Geissel, M. Hegelich, H. Pépin, H. Popescu, H. Renard-LeGalloudec, M. Roth, J. Schreiber, R. Stephens, and T.E. Cowan, Phys. Rev. Lett. **94**, 045004 (2005).

13 J. Fuchs, P. Audebert, M. Borghesi, H. Pépin, and Oswald Willi, C. R. Physique **10**, 176 (2009).

14 A. Mancic. J. Robiche, P. Antici, P. Audebert, C. Blancard, P. Combis, F. Dorchies, G. Faussurier, S. Fourmaux, M. Harmand, R. Kodama, L. Lancia, S. Mazevet, M. Nakatsutsumi, O. Peyrusse, V. Recoules, P. Renaudin, R. Shepard, and J. Fuchs, High Energy Density Physics **6**, 21 (2010).

15 J.F. Ziegler, J.P. Biersack, and U. Littmark, *The Stopping and Range of Ions in Solids*, Pergamon Press, 1996.

16 J.B. Marion and J.L. Fowler. *Fast Neutron Physics,* Interscience Publishers, 1960.

17 G.A. Mourou, C.L. Labaune, M. Dunne, N. Naumova, and V.T. Tikhonchuk, Plasma Phys. Control. Fusion **49**, B667 (2007).

18 J. Fuchs, P. Antici, E. D'Humières, E. Lefebvre, M. Borghesi, E. Brambrink, C. A. Cecchetti, M. Kaluza, V. Malka, M. Manclossi, S. Meyroneinc, P. Mora, J. Schreiber, T. Toncian, H. Pépin, and P. Audebert, Nature Phys. **2**, 48 (2006).

19 J. Davis, G.M. Petrov, Tz Petrova, L. Willingale, A Maksimchuk, and K. Krushelnick, Plasma Phys. Control. Fusion **52**, 045015 (2010).

Table I. Comparison of conventional sources of neutron production with ultra-intense laser facility capabilities. Yields represent “on target” neutron flux, for which the laser facilities assume a 1m distant target, 20° divergent neutrons, and 1Hz repetition rate for LULI and 1/60 Hz repetition for ELI.

Source	Yield	Energy	Timescale	FWHM
Spallation(SNS)	10^{8}n/cm^{2}s	eV	μs	-
Fission(HFIR)	10^{15}n/cm^{2}s	eV	steady	-
Commercial(DD/DT – SODERN)	10^{6}n/cm^{2}s	3.5-14 MeV	steady	-
TW Lasers (LULI)	10^{4}n/cm^{2}s	10 MeV	ps	21°
EW Lasers (ELI) – Max	10^{7}n/cm^{2}s	200 MeV	ps	19°

Figure Captions

FIG. 1 (Color online): Schematic of the dual target configuration. A laser pulse accelerates deuterium ions from the primary target (e.g. 20 um Au with rear D layer) towards the secondary target (e.g. 25mm CD_2) to create neutrons through fusion events in the secondary target.

FIG. 2 (Color online): (a) Angle and energy (b: 0°, c: 90°) distributions of emitted neutrons for monoenergetic, normally incident ions of energy .1 MeV(solid), 1 MeV (dot), and 10 MeV (dash). Plots linearly scaled individually such that the maximum neutron emission in the angular and 0° plots are unity. Total yields: 0.1 MeV – 6.8×10^{-8} n/ion, 1 MeV – 8.8×10^{-6} n/ion, 10MeV – 5.1×10^{-4} n/ion. Yields in the forward direction (for comparison with [4]): 0.1 MeV – 1.0×10^{-8} n/sr/ion, 1 MeV – 2.2×10^{-6} n/sr/ion, 10MeV – 4.3x10-4 n/sr/ion.

FIG. 3 (Color online): Monte-Carlo calculated neutron yields from the LULI (dashed) and Trident (solid) lasers as a function of (a) angle and energy in the (b) 0° and (c) 90° directions.

FIG. 4 (Color online): **All)** Dashed corresponds to $I=1.6 \times 10^{23}$ W/cm^2 and solid to $I=1.6 \times 10^{21}$ W/cm^2. Secondary target thickness = 25mm. **a)** Calculated deuteron spectrum achievable at the ELI laser facility using the scaling in Ref. [18]. **b)** Projected angular neutron distribution. **c)** Neutron energy distribution at 0° and **d)** 90°

FIG. 5 (Color online): Schematic of microlens focusing technique [11]. Divergent deuterons are focused using a hollow cavity excited by a laser pulse. The resulting neutrons from the secondary target are consequently less divergent than without the microlens.

FIG. 6 (Color online): Energy distribution at a) 0° and b) 90° of neutrons emitted from thin (20 μm) targets with incident ion energies of 1 MeV (solid) 10 MeV(dotted) and 50 MeV(dashed).

FIG. 7 (Color online): (a,b) Incident ion and (c,d) emergent neutron energy distributions for thin (20 μm) targets and microlens focusing. (a,c): $6x10^{19}$ W/cm^2 LULI spectrum with a microlens centered at 12 MeV and selection width of 0.1 MeV. (b,d): Moderate ELI spectrum with a microlens centered at 200 MeV and selection width of 5 MeV.

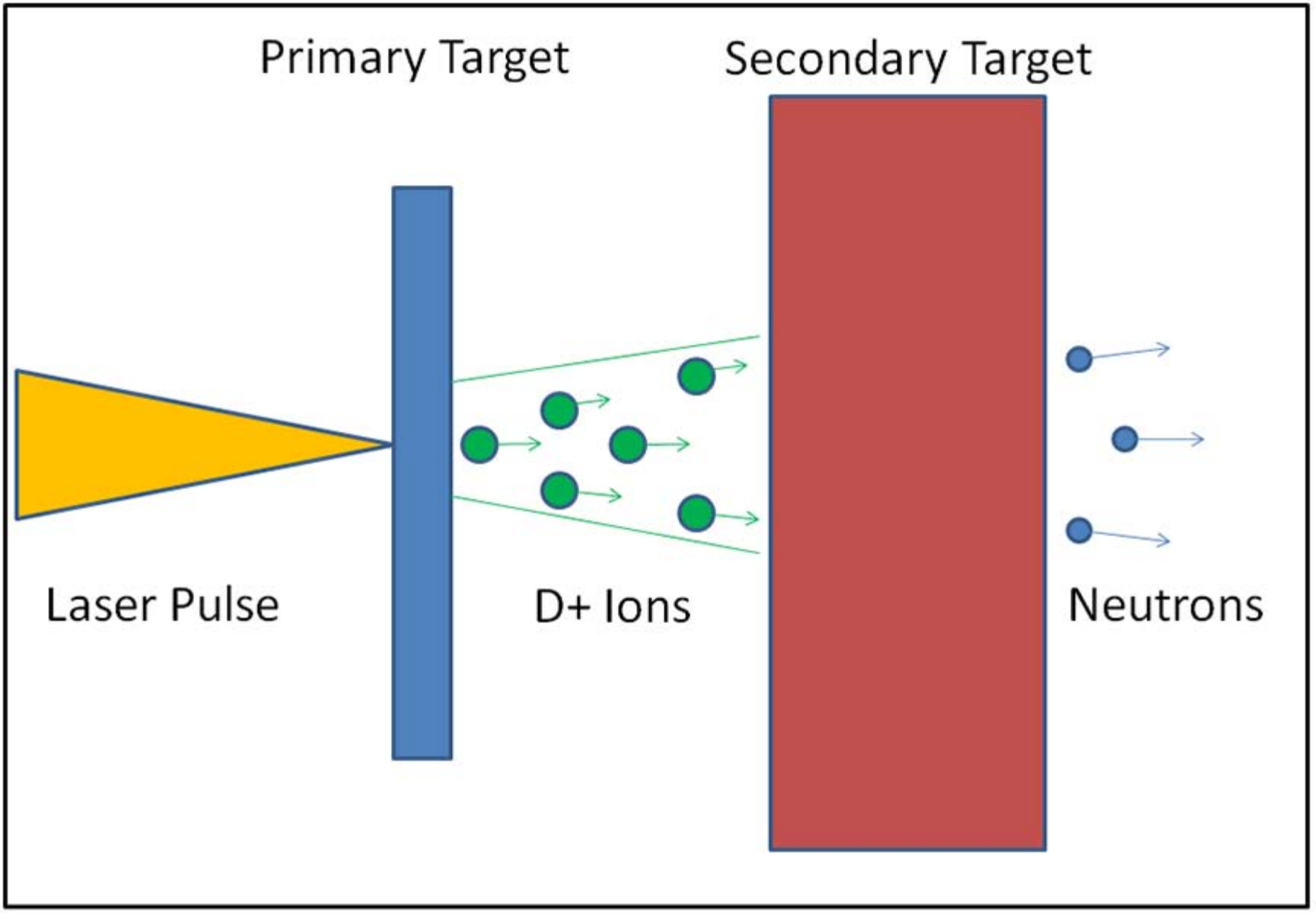
Primary Target
Secondary Target
Laser Pulse
D+ Ions
Neutrons

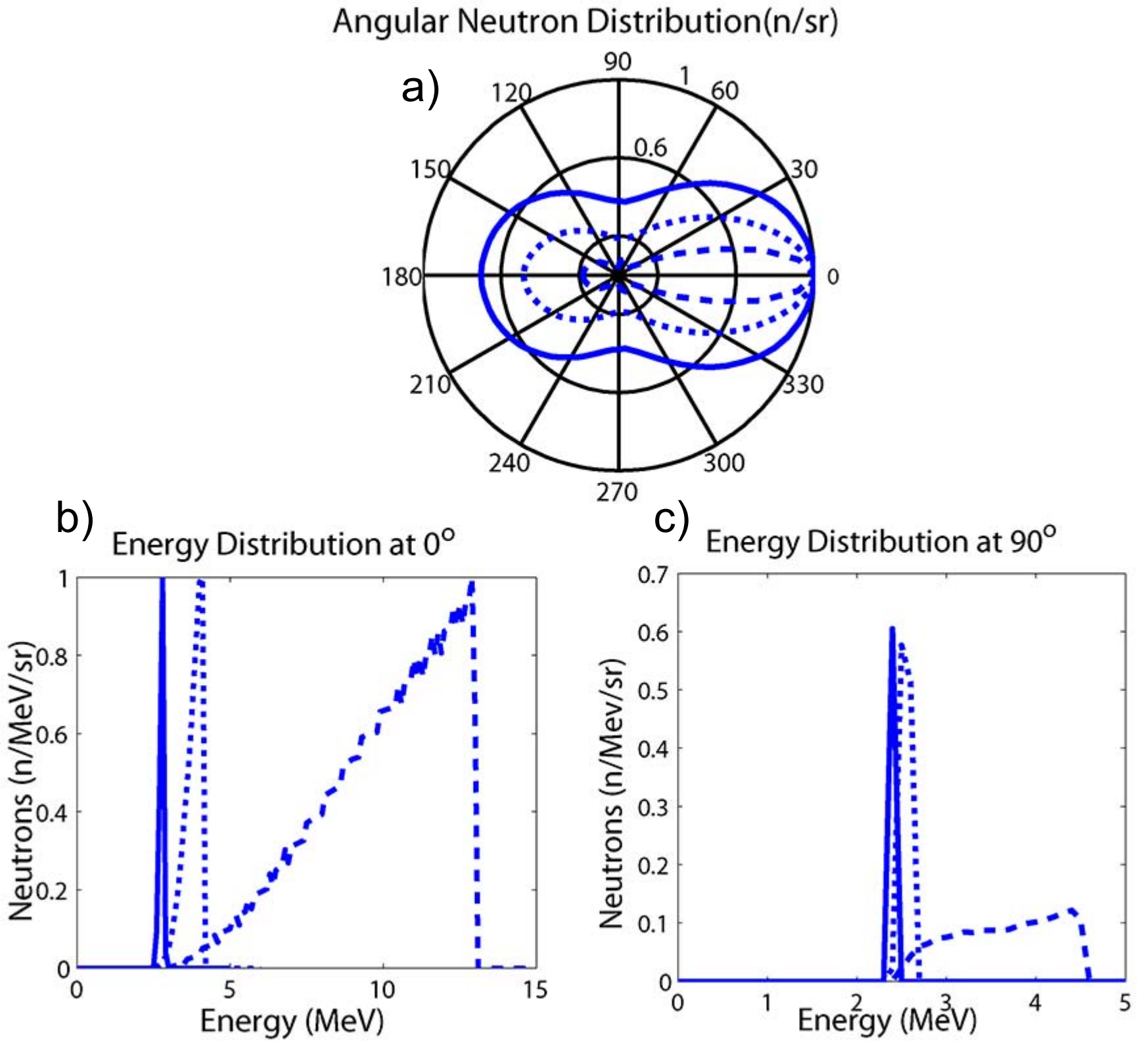
Angular Neutron Distribution(n/sr)
a)
90
1
60
120
0.6
150
30
180
0
210
330
240
300
270
b)
Energy Distribution at 0°
Neutrons (n/MeV/sr)
Energy (MeV)
c)
Energy Distribution at 90°
Neutrons (n/Mev/sr)
Energy (MeV)

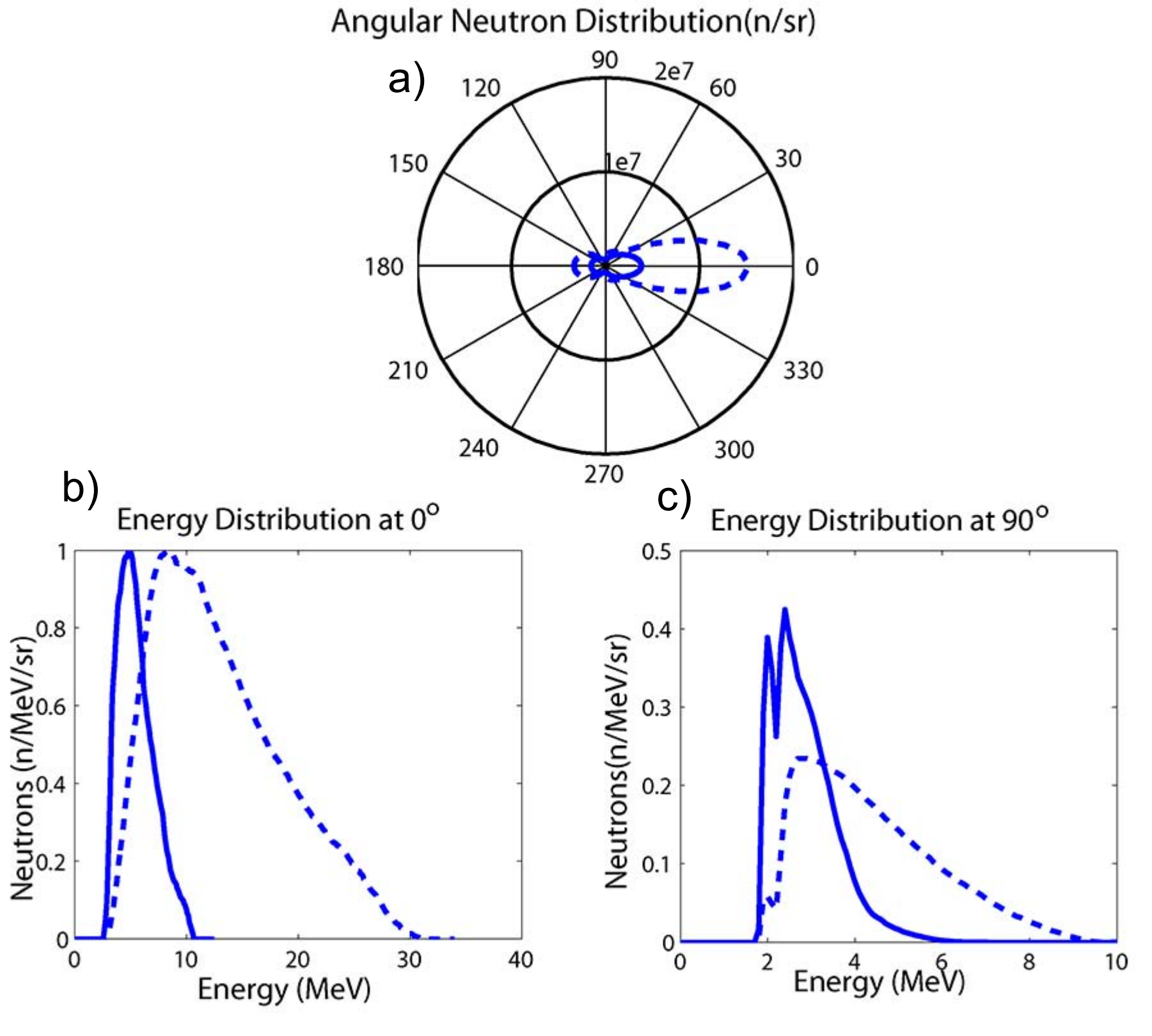
Angular Neutron Distribution(n/sr)
a)
90
2e7
60
120
30
150
1e7
180
0
210
330
240
300
270
b)
Energy Distribution at 0°
Neutrons (n/MeV/sr)
Energy (MeV)
c)
Energy Distribution at 90°
Neutrons(n/MeV/sr)
Energy (MeV)

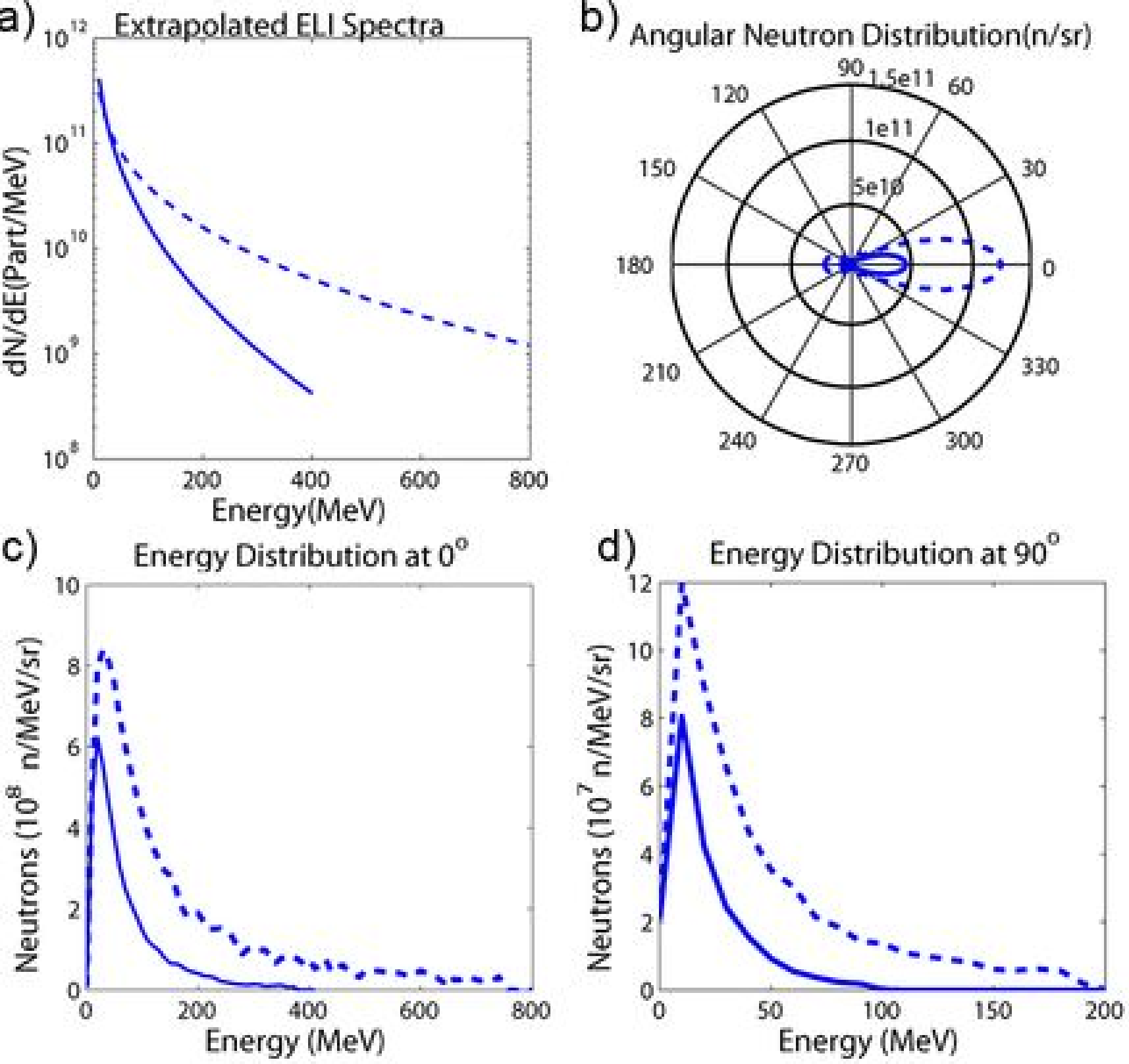
a)
Extrapolated ELI Spectra
dN/dE(Part/MeV)
Energy(MeV)
b)
Angular Neutron Distribution(n/sr)
1.5e11
1e11
5e10
c)
Energy Distribution at 0°
Neutrons (10^8 n/MeV/sr)
Energy (MeV)
d)
Energy Distribution at 90°
Neutrons (10^7 n/MeV/sr)
Energy (MeV)

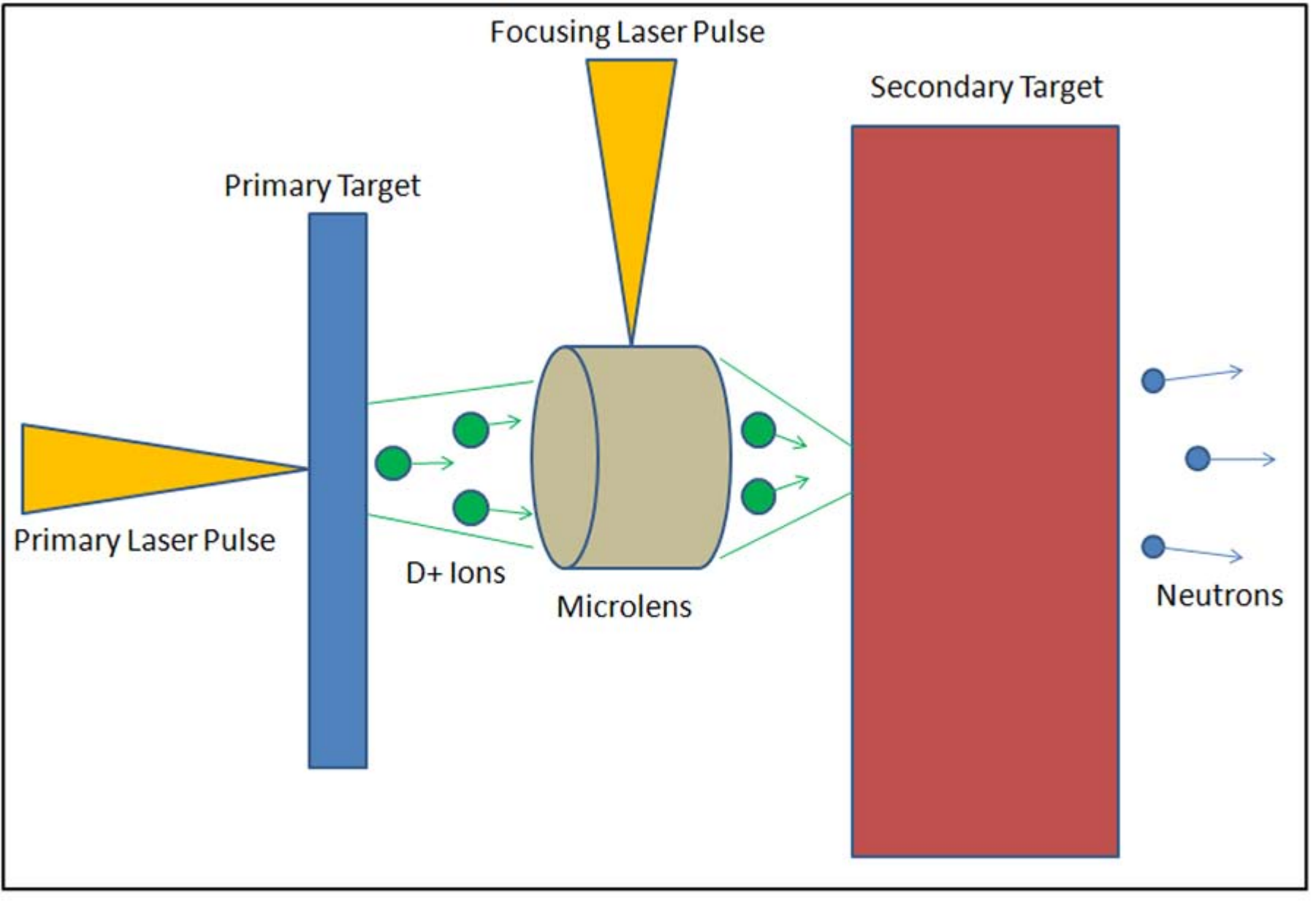
Focusing Laser Pulse
Secondary Target
Primary Target
Primary Laser Pulse
D+ Ions
Microlens
Neutrons

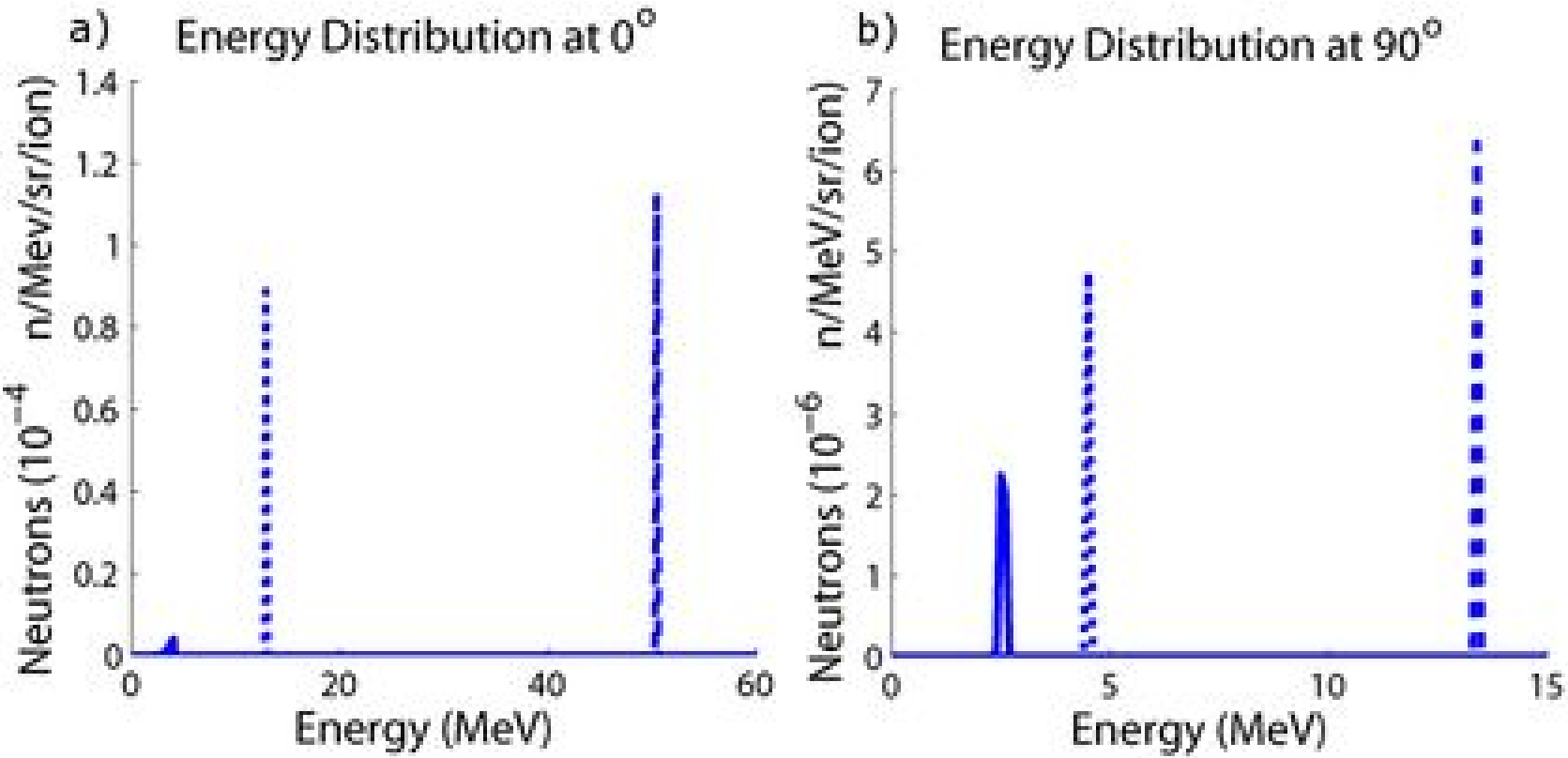
a)
Energy Distribution at 0°
Neutrons (10^{-4} n/Mev/sr/ion)
1.4
1.2
1
0.8
0.6
0.4
0.2
0
0
20
40
60
Energy (MeV)
b)
Energy Distribution at 90°
Neutrons (10^{-6} n/MeV/sr/ion)
7
6
5
4
3
2
1
0
0
5
10
15
Energy (MeV)

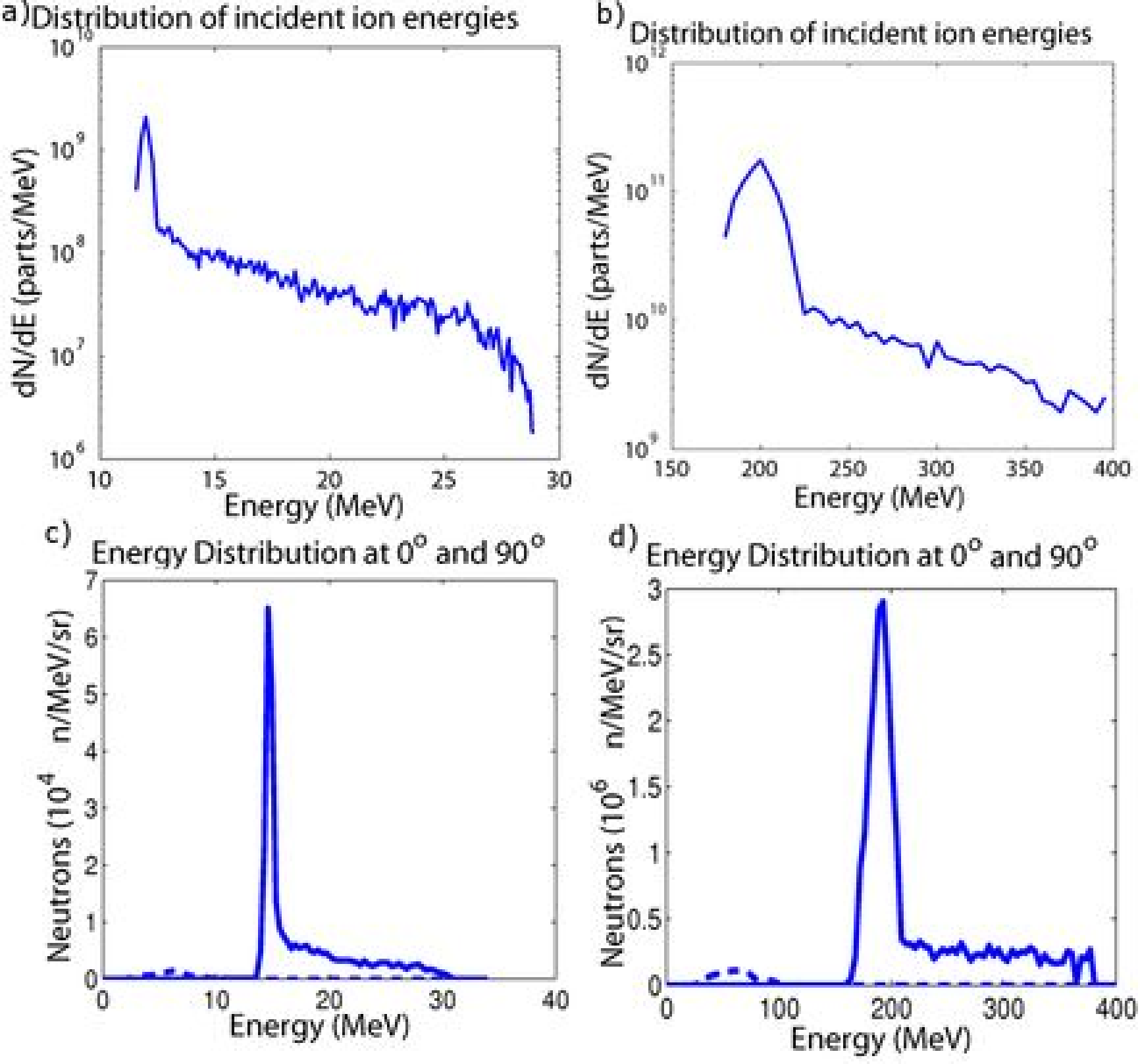
a) Distribution of incident ion energies
dN/dE (parts/MeV)
Energy (MeV)
b) Distribution of incident ion energies
dN/dE (parts/MeV)
Energy (MeV)
c) Energy Distribution at 0° and 90°
Neutrons (10^4 n/MeV/sr)
Energy (MeV)
d) Energy Distribution at 0° and 90°
Neutrons (10^6 n/MeV/sr)
Energy (MeV)

The Princeton Plasma Physics Laboratory is operated
by Princeton University under contract
with the U.S. Department of Energy.

Information Services
Princeton Plasma Physics Laboratory
P.O. Box 451
Princeton, NJ 08543

Phone: 609-243-2245
Fax: 609-243-2751
e-mail: pppl_info@pppl.gov
Internet Address: http://www.pppl.gov